NANO LETTERS

Letter

pubs.acs.org/NanoLett

Auxetic Black Phosphorus: A 2D Material with Negative Poisson's Ratio

Yuchen Du,[†,§] Jesse Maassen,[*,†,§,∥] Wangran Wu,[†,§] Zhe Luo,[‡,§] Xianfan Xu,[*,‡,§] and Peide D. Ye[*,†,§]

[†]School of Electrical and Computer Engineering, Purdue University, West Lafayette, Indiana 47907, United States

[‡]School of Mechanical Engineering, Purdue University, West Lafayette, Indiana 47907, United States

[§]Birck Nanotechnology Center, Purdue University, West Lafayette, Indiana 47907, United States

[∥]Department of Physics and Atmospheric Science, Dalhousie University, Halifax, Nova Scotia B3H 4R2, Canada

Supporting Information

ABSTRACT: The Poisson's ratio of a material characterizes its response to uniaxial strain. Materials normally possess a positive Poisson's ratio - they contract laterally when stretched, and expand laterally when compressed. A negative Poisson's ratio is theoretically permissible but has not, with few exceptions of man-made bulk structures, been experimentally observed in any natural materials. Here, we show that the negative Poisson's ratio exists in the low-dimensional natural material black phosphorus and that our experimental observations are consistent with first-principles simulations. Through applying uniaxial strain along armchair direction, we have succeeded in demonstrating a cross-plane interlayer negative Poisson's ratio on black phosphorus for the first time. Meanwhile, our results support the existence of a cross-plane intralayer negative Poisson's ratio in the constituent phosphorene layers under uniaxial deformation along the zigzag axis, which is in line with a previous theoretical prediction. The phenomenon originates from the puckered structure of its in-plane lattice, together with coupled hinge-like bonding configurations.

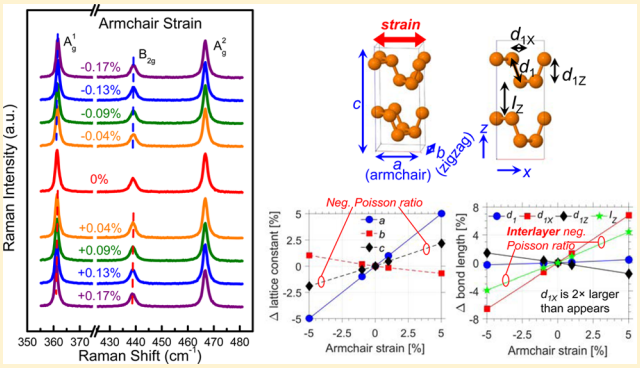

KEYWORDS: *black phosphorus, negative Poisson's ratio, strain, Raman spectroscopy, DFT calculations*

When a material is stretched in one direction by ΔL, as depicted in Figure 1a, it usually tends to contract in the other two directions perpendicular to the direction of stretching. Similarly, when a material experiences a compressive force, it expands laterally in the directions perpendicular to the direction of compression.[1,2] In both cases, the magnitude of deformation is governed by one of the fundamental mechanical properties of materials, the so-called Poisson's ratio. The Poisson's ratio of a material defines the ratio of the transverse contraction to the longitudinal extension in the direction of the stretching force. Specifically, it quantitatively explains how much a material becomes thinner (or thicker) in lateral directions when it experiences a longitudinal tension (or compression).[1,2] For ordinary materials, the Poisson's ratio is always positive. However, the possibility that the Poisson's ratio becomes negative has been an accepted concept in the classical elasticity theory for over 160 years,[1,3] implying that a material with a negative Poisson's ratio would undergo a transverse contraction when compressed and a transverse expansion when stretched in the longitudinal direction. Although a negative Poisson's ratio is theoretically permitted, direct observation of such a phenomenon in natural materials has never happened. Materials with a negative Poisson's ratio, also named auxetic materials, were demonstrated in 1987 by Lakes in a designed re-entrant (bow-tie) form.[4] Since then, auxetic materials have been extensively studied in macroscopic bulk form with microscopically engineered structures, as they can be useful in medicine, tissue engineering, bulletproof vests, and fortified armor enhancement. The negative Poisson's ratio in these man-made structures is derived from controlling the geometry and deformation mechanism of the internal material structure from the macroscopic level down to the molecular level.[1,5−10] Although the concept of auxetic materials with special artificial microstructures has gradually become accepted within the past decades, the question remains whether a negative Poisson's ratio exists in natural materials. In fact, theoretical predictions of a negative Poisson's ratio in naturally occurring single crystal was proposed back in the early 70s[11,12] and also performed on a variety of crystal models.[13−18] However, there is a lack of experimental evidence since the measurement of internal deformation in auxetic materials, in particular at the atomic level, is extremely difficult. In practice, the in-plane Poisson's

Received: August 26, 2016
Revised: September 17, 2016
Published: September 20, 2016

DOI: 10.1021/acs.nanolett.6b03607
Nano Lett. 2016, 16, 6701−6708

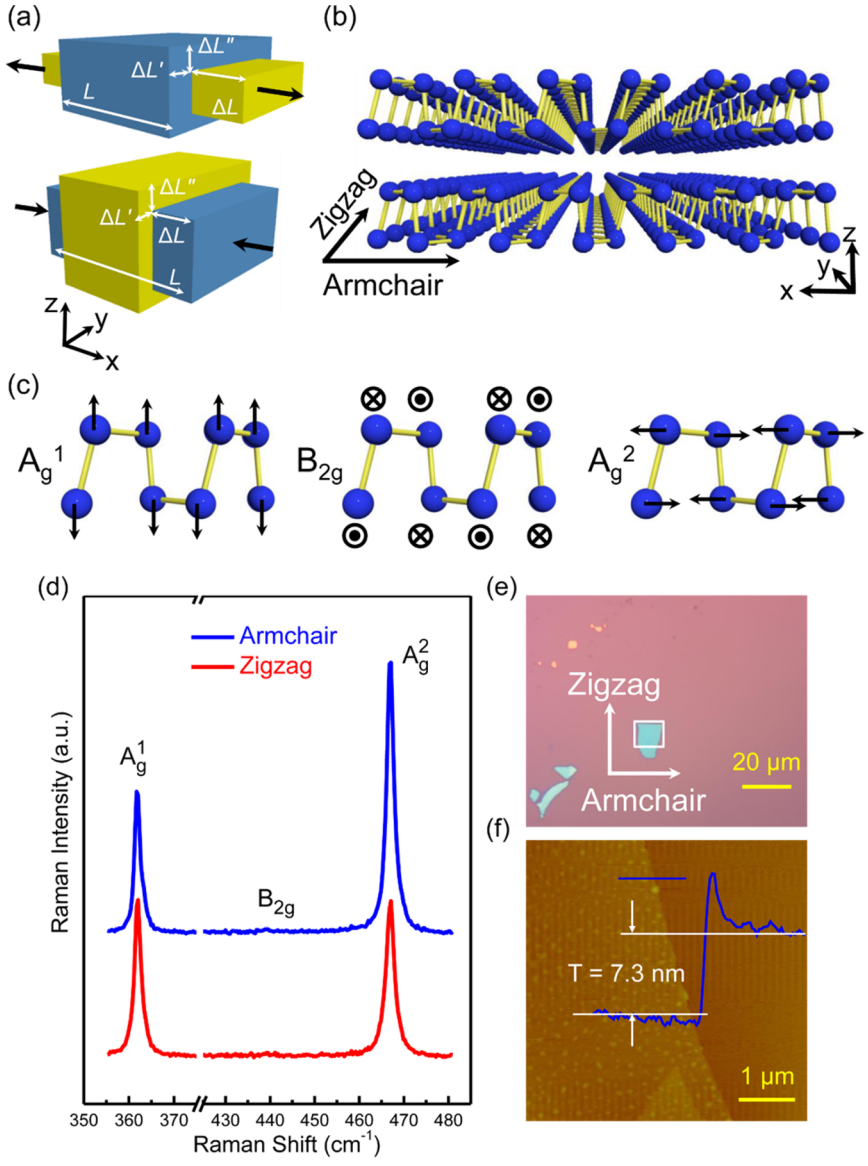

Figure 1. BP characterization. (a) Schematic view of the positive Poisson's effect. A cube with sides of length L of an anisotropic linearly elastic material subject to both tensile and compressive strains along x axis. The blue box is unstrained. The yellow box is stretched (compressed) in the x direction by ΔL, and contacted (expanded) in the y and z directions by $\Delta L'$ and $\Delta L''$, respectively. (b) Lattice structure of BP and (c) atomic vibrational patterns of A_g^1, B_{2g}, and A_g^2 phonon modes. (d) Polarized Raman spectra of BP to distinguish the armchair and zigzag axes. The armchair direction has A_g^2/A_g^1 intensity ratio of ~2, whereas the zigzag direction has a ratio of ~1. (e) Optical image of the 7.3 nm thick BP flake with two principle lattice orientations. The white box indicates the laser focusing location. Scale bar in optical image is 20 μm. (f) AFM topology of measured BP flake, and the scale bar is 1 μm.

ratio measurement was conducted by recording the movements of location markers on a surface during constant-rate deformation, and the cross-plane Poisson's ratio was obtained from utilizing scanning electron microscopy to generate vertical distance variations with applied in-plane strains.[19] Even though previous efforts have been carried out in studying the auxetic behavior among man-made materials and structures, we are not aware of any reports on the experimental demonstration of the negative Poisson's ratio in naturally occurring crystals at atomic structure accuracy as we present here on a 2D auxetic material—black phosphorus (BP).

BP, a stable phosphorus allotrope at room temperature,[20] is a layered natural semiconducting crystal composed of sheets of monolayer phosphorene, and therefore, it can be mechanically exfoliated into atomically thin layers with a vertical dimension of a couple of nanometers down to one monolayer.[21−29] The importance of exploring isolated thin-film BP is built on the fact that it bridges the gap between zero bandgap graphene and wide bandgap transition metal dichalcogenides, thereby providing a new route to expand the scope of experimentally accessible 2D crystals, and pursue a broad range of the fundamental studies. BP exhibits a thickness-dependent bandgap characteristic, ranging from ~0.3 eV in bulk crystal to >1.4 eV in the form of a monolayer.[21−26] Its p-type nature and high carrier mobility are also valuable contributions to the family of 2D materials. The moderate bandgap, along with relatively high carrier mobility, also benefits BP in electronic and optoelectronic applications.[21−29] Here, we focus on another property of BP: its unique puckered structure allows BP to exhibit substantial anisotropy in the mechanical

DOI: 10.1021/acs.nanolett.6b03607
Nano Lett. 2016, 16, 6701−6708

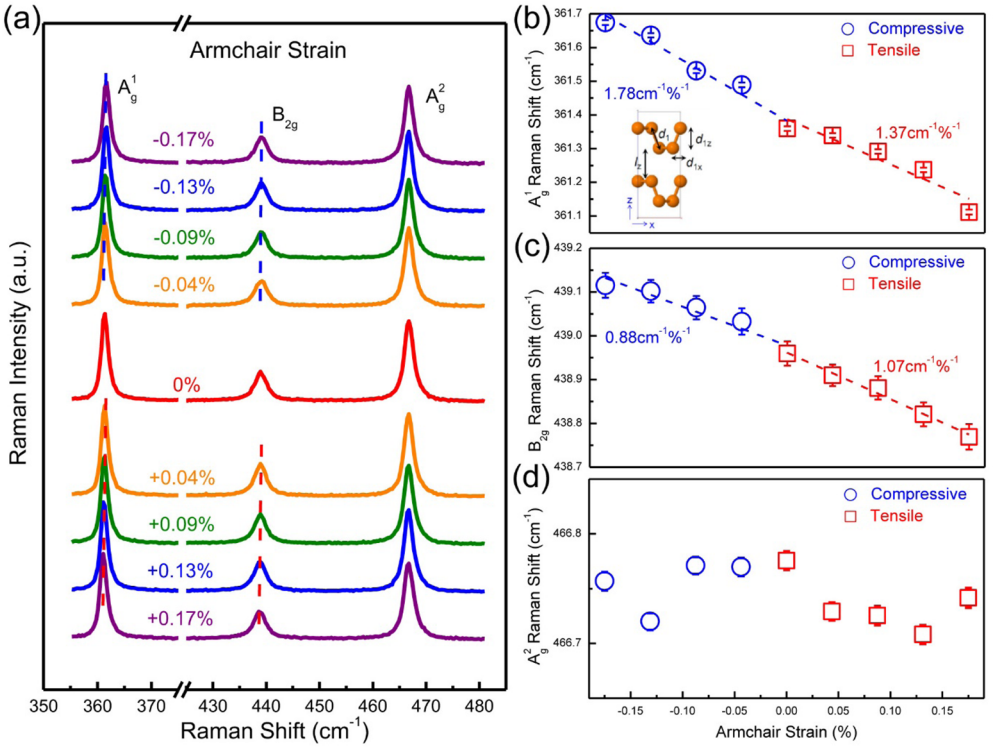

Figure 2. Raman evolution of uniaxial armchair strained BP. (a) Raman spectra of BP for both tensile and compressive armchair strains. The dashed lines are here to guide the Raman peak position shift. Raman shift of (b) A_g^1, (c) B_{2g}, (d) A_g^2 modes in armchair strained BP. The dashed lines show linear fit results, and error bars are determined from Lorentzian peak fittings.

properties with respect to strains[30−39] and encourages us to experimentally and theoretically investigate and demonstrate the existence of negative Poisson's ratio.

In this study, we employed Raman spectroscopy to experimentally demonstrate the cross-plane interlayer (between adjacent monolayer phosphorene layers) negative Poisson's ratio when it is uniaxially strained along the armchair direction. Furthermore, we confirmed the existence of the cross-plane intralayer (within a monolayer phosphorene layer) negative Poisson's ratio under uniaxial deformation along the zigzag direction. In contrast to man-made bulk structures, these multiple negative Poisson's ratios are intrinsic to BP, and they are attributed to the puckered structure along its in-plane anisotropic axes, where the unique lattice structure can be regarded as a natural re-entrant form that is comprised of two coupled hinge-like bonding configurations.[36]

Results. *Lattice Vibration Modes and Polarized Raman Characterization of BP.* In a unit cell of BP, each phosphorus atom covalently bonds to its three nearest neighbors, forming warped hexagons. As shown in Figure 1b, this sp^3-type bonding has introduced a distinctly anisotropic crystal structure resulting in two principal lattice axes referred to as armchair (x direction) and zigzag (y direction), which are perpendicular and parallel to the pucker, respectively.[21] The geometric anisotropy introduced by the pucker implies that BP would exhibit significant anisotropic lattice vibration response to uniaxial strain along armchair or zigzag directions,[36,37] which can be observed directly from Raman spectroscopy.[38,39] Previous studies of Raman spectra have shown that there are three prominent active modes in BP.[23,24] The cross-plane A_g^1 mode occurs due to opposing vibrations of top and bottom phosphorus atoms with respect to each other. The B_{2g} mode describes the bond movement along the in-plane zigzag direction. The A_g^2 mode has a dominant component along the in-plane armchair direction, as illustrated in Figure 1c. To start our experiment, few-layer BP was exfoliated from the bulk crystal by the standard scotch tape method and transferred to a conducting Si substrate with a 300 nm SiO_2 capping layer. Polarized Raman spectroscopy was utilized to determine the flake orientation.[29] With the detection polarization parallel to the incident laser polarization, the active phonon mode of B_{2g} is not detected due to matrix cancellation when the two principle lattice axes are aligned with the laser polarization.[29] The A_g^2/A_g^1 Raman intensity ratio can further be used to distinguish the specific armchair or zigzag axis. The intensity of the armchair-oriented A_g^2 mode is maximized and is about twice the intensity of the A_g^1 mode when the laser polarization is along the armchair direction. The intensity of A_g^2 is comparable to A_g^1 when laser is aligned along the zigzag direction.[29] The candidate BP flakes were all precharacterized by the polarized Raman system. Optical and atomic force microscope (AFM) images of a representative 7.3 nm thick BP flake are presented in Figure 1e and f, respectively. The armchair and zigzag lattice axes in Figure 1e were determined by the A_g^2/A_g^1 intensity ratio shown in Figure 1d.

Interlayer Negative Poisson's Ratio in Armchair Strained BP. We first investigate the evolution of the Raman spectra of BP with uniaxial tensile and compressive strains, summarized in Figure 2a. The laser polarization is aligned along the zigzag axis of BP flake, and the strain direction is along armchair direction based on our apparatus setup (see Supporting Information Note 1). In our work, we used Lorentzian functions to fit the Raman spectra and obtained the peak frequency of each mode at different strains. For unstrained BP, consistent with previous reports,[23,24] we observe the cross-plane vibration mode of A_g^1 at ~362 cm^{-1}, and in-plane vibration modes of B_{2g} and A_g^2 at

DOI: 10.1021/acs.nanolett.6b03607
Nano Lett. 2016, 16, 6701−6708

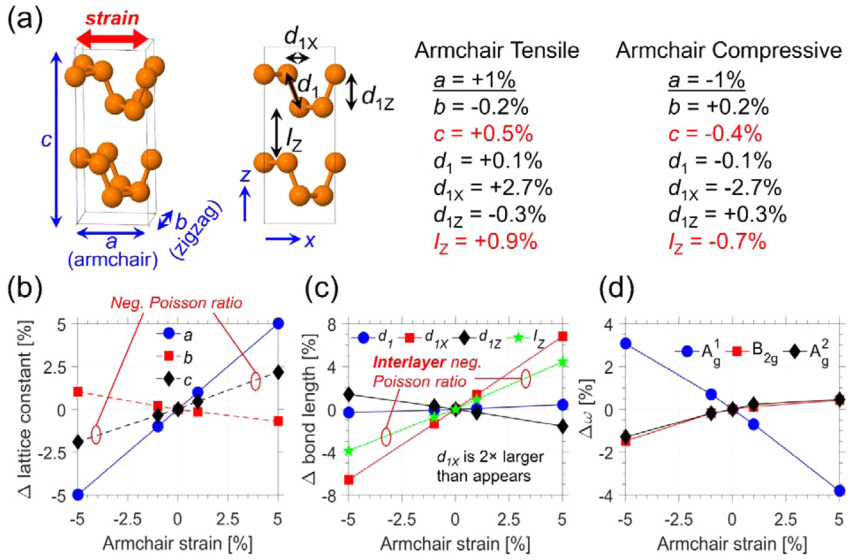

Figure 3. Simulation of armchair strained BP. (a) Atomic structure of bulk BP. The lattice constants along the main crystals directions are indicated with blue arrows. The cross-plane bond (d_1), along with its x and z projections, and the interlayer distance (I_z) are indicated with black arrows. (b) Calculated variation in lattice constants due to uniaxial strain along the armchair direction. The solid line indicates the lattice parameter that is fixed to apply the strain. (c) Calculated variation in bond lengths due to uniaxial strain along the armchair direction. The d_{1X} projected bond length is twice as large as it appears, to more easily visualize the data in this figure. (d) Calculated variation in the A_g^1, B_{2g}, and A_g^2 phonon frequency due to uniaxial strain along the armchair direction. A positive strain value corresponds to stretching the BP lattice along the armchair direction, and a negative strain value corresponds to compressing the lattice.

~439 cm^{-1} and ~467 cm^{-1}, respectively. The A_g^1 and B_{2g} modes show the same linear trend of Raman frequency shift with respect to the applied strain, whereas the rate of frequency shift is different in these two modes. Both A_g^1 and B_{2g} modes experience a red shift when BP is under tensile strain along the armchair direction, with a slope of 1.37 cm^{-1} $\%^{-1}$ and 1.07 cm^{-1} $\%^{-1}$, respectively. On the other hand, A_g^1 and B_{2g} have a blue shift at a rate of 1.78 cm^{-1} $\%^{-1}$ and 0.88 cm^{-1} $\%^{-1}$ under uniaxial compressive strain, as shown in Figure 2b,c. It is worth mentioning that we did not observe a measurable Raman shift in the A_g^2 mode, corresponding to the lateral vibration in the armchair direction, with armchair strains (see Supporting Information Note 2), and we believe this can be attributed to the fact that the BP structure is anisotropic and is much softer along the armchair direction, compared to the zigzag direction. The sensitivity of determining strains in BP using Raman peak positions is greater than that of molybdenum disulfide (MoS_2), but slightly smaller than those of carbon nanotubes and graphene.[40,41] The error bars in the figures are extracted from the Lorentzian peak fittings, which are significantly smaller than the strain-induced frequency shift. For the applied strain less than 0.2%, the Raman peak position remains the same at each strain level after multiple loading and unloading cycles, indicating our experiments are highly reliable (see Supporting Information Note 3). In addition, the absence of discrete jumps of any of the three Raman modes under monotonically varied strains assures that the BP flake does not slip against the substrate during strain experiments.

The different responses of Raman spectra with strains can be explained by analyzing the types of vibration mode involved.[37] Let us take the A_g^1 mode as an example, where the atomic motions occur mainly along the cross-plane direction. As depicted in the inset of Figure 2b, the A_g^1 mode vibration in few-layer BP is determined by two components, the interlayer distance I_Z and the intralayer phosphorus bond length d_1. The red shift of the A_g^1 mode under tensile strain along the armchair direction, with a slope of 1.37 cm^{-1} $\%^{-1}$, can be understood on the basis of the elongation of the P−P intralayer bond length d_1, which weakens the interatomic interactions and therefore reduces the vibration frequency. Also, there exists another possibility that the red-shifted Raman frequency of the A_g^1 mode is attributed to the enlarged interlayer distance I_Z, where reduced interlayer interactions can also weaken the cross-plane vibration frequency.[42−46] If this is true, then it is interesting that BP expands (both intralayer bond length d_1 and interlayer distance I_Z) when it is stretched along the armchair direction, which is opposite to the definition of positive Poisson's ratio. Meanwhile, the blue shift of 1.78 cm^{-1} $\%^{-1}$ under compressive armchair strain indicates the intralayer bond length and interlayer distance may be smaller under compressive armchair strain, thus proposing a hypothesis that the cross-plane Poisson's ratio is negative in BP with an armchair full strain.

To corroborate our experimental findings that suggest a negative Poisson's ratio in the cross-plane direction and to determine the individual contributions from I_Z and d_1, we performed density functional theory (DFT) calculations of strained BP (details are described in the Methods section). Because the experimental thickness of the BP samples is ~7 nm, for our modeling purposes, we focus on bulk BP. Bulk BP is characterized by three lattice constants a, b, and c, aligned along the armchair, zigzag, and cross-plane directions, respectively (see Figure 3a). Figure 3b shows how the lattice constants are modified with uniaxial strains along the armchair directions. Interestingly, we also observe a negative Poisson's ratio from our DFT calculations: +1% tension (or −1% compression) of the armchair lattice parameter, a, enhances +0.5% (or reduces −0.4%) the cross-plane lattice parameter, c. In other words, BP becomes "thicker" in the vertical direction as it undergoes armchair tensile strain, and it becomes "thinner" in the vertical direction under armchair compressive strain. This

DOI: 10.1021/acs.nanolett.6b03607
Nano Lett. 2016, 16, 6701−6708

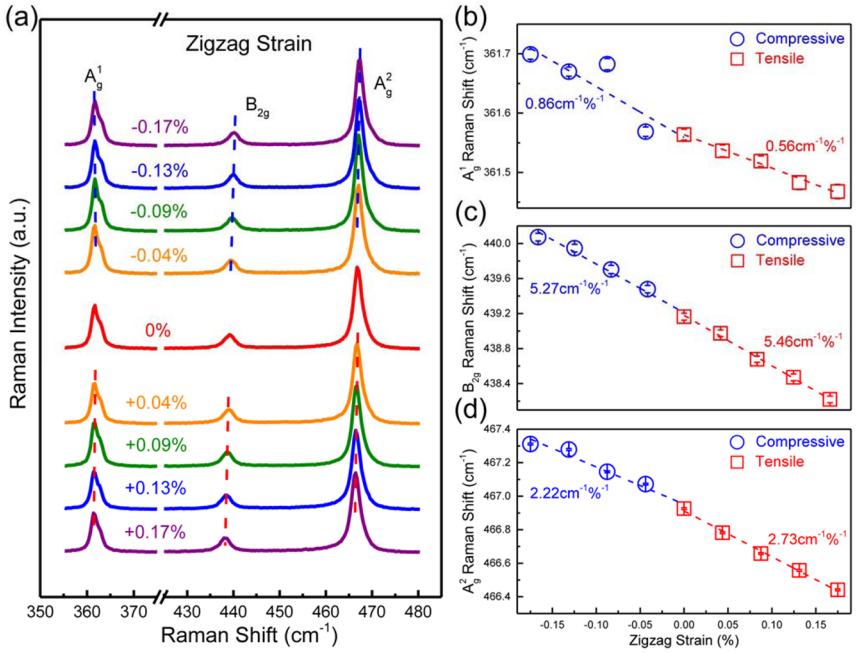

Figure 4. Raman evolution of uniaxial zigzag strained BP. (a) Raman spectra of BP for both tensile and compressive zigzag strains. The dashed lines are here to guide the Raman peak position shift. Raman shift of (b) A_g^1, (c) B_{2g}, and (d) A_g^2 modes in zigzag strained BP. The dashed lines show linear fit results, and error bars are determined from Lorentzian peak fitting.

supports the hypothesis derived from the experimental observation that the cross-plane Poisson's ratio is negative for the entire armchair strain. The value of the Poisson's ratio, defined as $\nu \approx -\frac{\Delta L'}{\Delta L}$, where $\Delta L'$ and ΔL are the variation in the cross-plane direction and in the armchair direction, respectively, are thus −0.5 under tension and −0.4 under compression. Note that the magnitude of the strain values assumed in the calculations is equal to or larger than 1% to ensure accurate results well above the numerical error.

To understand the origin of how the cross-plane lattice parameter c is modified with strain, in Figure 3c, we present how the various atomic distances, and their projections, are modified due to armchair strain. The lattice parameter c is controlled by both the z projection of the cross-plane P−P bond d_{1Z} and the interlayer distance I_Z. The intralayer d_{1Z} shows a regular positive Poisson's ratio, meaning the constituent monolayer phosphorene layers flatten (or expand) when stretched (or compressed) laterally along the armchair direction. This is consistent with previous calculations of armchair strain in monolayer phosphorene.[36] However, the interlayer I_Z shows an unusual negative Poisson's ratio behavior, where the distance between the monolayer phosphorene layers expands by +0.9% (or shrinks by −0.7%) when stretched (or compressed) laterally along the armchair direction by 1%. More importantly, the change in I_Z under armchair strain is more pronounced than that of d_{1Z}, meaning the cross-plane lattice parameter c is dominated by the interlayer distance I_Z rather than d_{1Z}. Thus, the negative Poisson's ratio associated with c originates from the interlayer coupling in BP, and we call this phenomenon interlayer negative Poisson's ratio, which is the first such demonstration in a naturally occurring 2D material. This also suggests that the interlayer interaction is not purely van der Waals in BP, but may also arise from the coupling between the wave functions of lone pair electrons in adjacent layers.[43,47,48] Naturally, this result was not predicted from the previous phosphorene studies,[36] which only considers a single layer, but did find a negative Poisson's ratio for d_{1Z} with zigzag strain (to be discussed in the following section). Within a small magnitude of strain, the first-order negative Poisson's ratio approximation yields,$\nu \approx -\frac{\Delta L'}{\Delta L}$ where ΔL and $\Delta L'$ are lattice constant variation and bond length variation with respect to armchair lattice and interlayer distance I_Z. Specifically, BP demonstrates an interlayer negative Poisson's ratio of −0.9 along stretching armchair, and −0.7 under armchair compression from DFT calculations.

To connect the strain induced atomic structural change to that of the Raman response, we calculated the phonons frequencies of bulk BP under strain. In Figure 1c, we show the atomic displacements associated with the three Raman-active phonon modes, A_g^1, B_{2g}, and A_g^2. As noted above, the A_g^1 mode corresponds to atomic motion predominantly in the cross-plane direction, and is thus likely to be most sensitive to variations in cross-plane distances (i.e., d_{1Z} and I_Z). Figure 3d presents the variation in phonon frequency versus armchair strain. Focusing on the A_g^1 mode, we find that the frequency increases with increasing armchair compressive strain. From a microscopic point of view, this can be understood as follows: when BP is compressed along armchair, the main effect is to modify the d_1 bond angle such that it aligns more with the cross-plane direction (in Figure 3c we see a large change in d_{1X} with little change to d_1). In this process, the d_1 bond becomes more closely aligned with the atomic displacement of the A_g^1 mode, which leads to an increase in A_g^1 frequency. With tensile armchair strain, the d_1 bond becomes less aligned with the atomic displacements of the A_g^1 mode and the energy decreases. This effect of bond angle alignment influences both the P atoms within a single layer (intralayer) and the nearest P atoms in adjacent layers (interlayer). Note that, interestingly, as the atoms in adjacent layers are brought closer through a modification of the d_1 bond angle via compressive armchair strain I_Z decreases, which enhances interlayer vibration and also increase A_g^1 frequency. Though we find

DOI: 10.1021/acs.nanolett.6b03607
Nano Lett. 2016, 16, 6701−6708

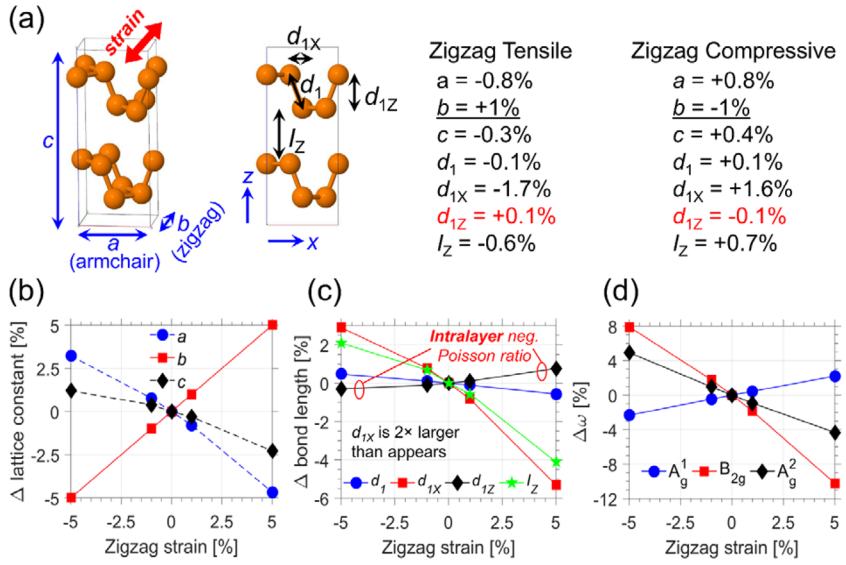

Figure 5. Simulation of zigzag strained BP. (a) Atomic structure of bulk BP. The lattice constants along the main crystals directions are indicated with blue arrows. The cross-plane bond (d_1), along with its x and z projections, and the interlayer distance (l_z) are indicated with black arrows. (b) Calculated variation in lattice constants due to uniaxial strain along the zigzag direction. The solid line indicates the lattice parameter that is fixed to apply the strain. (c) Calculated variation in bond lengths due to uniaxial strain along the zigzag direction. The d_{1X} projected bond length is twice as large as appears, to more easily visualize the data in this figure. (d) Calculated variation in the A_g^1, B_{2g}, and A_g^2 phonon frequency due to uniaxial strain along the zigzag direction. A positive strain value corresponds to stretching the BP lattice along the zigzag direction, and a negative strain value corresponds to compressing the lattice.

reasonable agreement with A_g^1, there is some discrepancy for the B_{2g} and A_g^2 modes. For example, we observe an opposite change in B_{2g} phonon energy with strain compared to experiment. We note, however, that the strain effect is relatively small. We believe that this difference could arise from the interaction of BP with the substrate, which is not captured in the calculations, or due to the larger adopted strain values in the DFT modeling (>1% theory versus <0.2% experiment). Nevertheless, the calculated changes in atomic structure due to strain, which are typically more robust than the more sensitive changes in phonon energy, show a negative Poisson's ratio. Thus, overall our theoretical results on the effect of strain on the atomic structure and the phonon energies are in good agreement with experimental data, supporting the existence of interlayer negative Poisson's ratio in layered BP along armchair uniaxial strain. This property is significantly different from other 2D materials, that is, MoS_2.[40,49]

Intralayer Negative Poisson's Ratio in Zigzag Strained BP. To apply strain along the zigzag direction, the same BP sample substrate was rotated by 90°, and the polarized Raman spectra was applied again to verify the BP orientation. The incident polarized laser light is aligned along the armchair direction. The corresponding Raman spectra of zigzag strained BP are presented in Figure 4a. Figure 4b illustrates the A_g^1 peak position as a function of tensile and compressive zigzag strain. The dominant A_g^1 mode peak overlaps with another peak appearing as a weak shoulder. In this case, we fitted the data by two Lorentzian functions and treated the main peak as the peak for the A_g^1 mode. This phenomenon only happens when the incident polarized light is along the armchair lattice of BP flakes, and it has been observed in our previous studies as well.[29] The A_g^1 mode shows a monotonic behavior for the full range of zigzag strain with a slope of 0.56 cm^{-1} $\%^{-1}$ under tensile strain and 0.86 cm^{-1} $\%^{-1}$ under compressive strain. On the other hand, we observe a much more pronounced B_{2g} and A_g^2 sensitivity with respect to the zigzag strain as compared to the armchair strain case. Specifically, B_{2g} sensitivities under tensile (5.46 cm^{-1} $\%^{-1}$) and compressive (5.27 cm^{-1} $\%^{-1}$) zigzag strains are 5−6 times larger than those under armchair strains. Meanwhile, the peaks of the A_g^2 mode also shift under zigzag strains, with about 2.73 cm^{-1} $\%^{-1}$ and 2.22 cm^{-1} $\%^{-1}$ for tensile and compressive strains, respectively. This giant anisotropic strain response in BP is directly associated with its anisotropic lattice structure, where the armchair axis is much softer with a smaller Young's modulus as compared to the zigzag axis. A previous theoretical study has predicted a negative Poisson's ratio in monolayer phosphorene along the cross-plane direction under uniaxial zigzag deformation.[36] Here, our DFT simulations of bulk BP also show a negative cross-plane intralayer Poisson's ratio for the zigzag strained BP, summarized in Figure 5a. Figure 5c shows that the calculated thickness of the constituent monolayer phosphorene layers, d_{1Z}, increases by +0.1% with 1% zigzag stretching and decreases by −0.1% with 1% zigzag compression, demonstrating an intralayer negative Poisson's ratio. Therefore, if we consider the intralayer deformation only, its Poisson's ratio is approximately −0.1 under zigzag strain, which is consistent with the previous report on monolayer phosphorene.[36] However, the interlayer distance l_Z shows a positive Poisson ratio characteristic (see Figure 5c) that counteracts the effect of d_{1Z}, thus leading to an overall positive Poisson's ratio for the lattice constant c with zigzag strain (see Figure 5b). The calculated variations in the B_{2g} and A_g^2 phonon frequency due to zigzag strain are given in Figure 5d. The sensitivity of the B_{2g} mode vs strain is nearly twice as high as that of the A_g^2 mode, agreeing well with the experimental results.

Conclusion. In summary, we have investigated the anisotropic strain responses of few-layer BP films under uniaxial tensile and compressive strains. For the first time, by examining the Raman evolution of uniaxially strained BP, we have succeeded in demonstrating a cross-plane negative Poisson's ratio when it is strained along the armchair direction. Ab initio

DOI: 10.1021/acs.nanolett.6b03607
Nano Lett. 2016, 16, 6701−6708

calculations have also been carried out to determine the influence of strain on the atomic structure of BP as well as on the phonon modes. Our theoretical results are consistent with experiment, and indicate there exists an interlayer negative Poisson's ratio between the phosphorene layers under armchair strain. Meanwhile, our results support the existence of a cross-plane intralayer negative Poisson's ratio in the constituent phosphorene layers under uniaxial deformation along the zigzag axis, which is in line with a previous theoretical prediction. In contrast to man-made auxetic materials, this is the first time a negative Poisson's ratio is observed experimentally in a natural material and confirmed by theoretical simulations.

Methods. *Sample Preparation.* Few-layer films were exfoliated from the bulk crystal BP (Smart-elements), and then transferred to a 525 μm thick Si substrate with a 300 nm SiO_2 capping layer. The thickness of the BP was measured using a Veeco Dimension 3100 AFM system. During the Raman measurement, the BP flake was exposed to the air for about 2 h, but with no significant degradation (see Supporting Information Note 4) in terms of lattice vibration modes.

Raman Measurements. All Raman measurements were carried out on a HORIBA LabRAM HR800 Raman spectrometer. The system is equipped with a He−Ne excitation laser (wavelength 632.8 nm), an 1800 g mm^{-1} grating, and a Nikon ×50 (NA = 0.45) long-working-distance objective lens. For polarized Raman characterization of the BP flakes, a linear polarizer (Thorlabs, LPNIRE050-B) was used as the analyzer. Subsequent Raman spectroscopy of strained BP studies was performed under an excitation laser power of 0.17 mW, sufficiently low to avoid excessive sample heating.

First-Principles Calculations. DFT calculations were carried out using the Vienna ab initio simulation package[50,51] (VASP), based on a plane-wave expansion of the wave functions and the projector augmented wave[52] (PAW) method to treat the effect of the core. Our calculations used the generalized gradient approximation (GGA) within the PBE approach for exchange-correlation potential. A plane-wave cutoff energy of 750 eV, and a Monkhorst−Pack k-grid of 17 × 23 × 23 were adopted to ensure proper convergence of the total energy (<10 μeV/atom). The simulation cell is defined by the following lattice vectors: $\boldsymbol{a}_1 = [a\ 0\ 0]$, $\boldsymbol{a}_2 = [0\ b/2\ -c/2]$, $\boldsymbol{a}_3 = [0\ b/2\ c/2]$, where the lattice constants are determined to be a = 4.564 Å, b = 3.305 Å, and c = 11.318 Å (in the case of no strain). In order to include the effect of uniaxial strain the lattice constant along the direction of strain was fixed, and the other two lattice constants were optimized to minimize the total energy (at each step the atoms were relaxed until the forces were <0.001 eV/Å). The Γ-point phonon mode energies/frequencies were calculated within the harmonic approximation using the finite displacement method to extract the second order force constants, as implemented in the Phonopy software package.[53] The force constants were obtained from 3 × 4 × 4 supercell self-consistent calculations using a 4 × 4 × 4 Γ-centered k-grid.

■ ASSOCIATED CONTENT

Supporting Information

The Supporting Information is available free of charge on the ACS Publications website at DOI: 10.1021/acs.nanolett.6b03607.

Additional details for four-point bending apparatus, air-stability of Raman spectra, layer-dependent strained BP, biaxial strained BP, and GGA/LDA simulation results. (PDF)

■ AUTHOR INFORMATION

Corresponding Authors

*E-mail: yep@purdue.edu (P.D.Y.).
*E-mail: xxu@ecn.purdue.edu (X.X.).
*E-mail: jmaassen@dal.ca (J.M.).

Author Contributions

P.D.Y. and X.X. conceived the idea, designed, and supervised the experiments. Y.D. and W.W. performed the strain experiments and analyzed the experimental data. J.M. conducted the theoretical calculations and analyses. Y.D., W.W., Z.L., and X.X. performed the polarized Raman experiments and analyses. Y.D., J.M., W.W., Z.L., X.X., and P.D.Y. cowrote the manuscript.

Notes

The authors declare no competing financial interest.

■ ACKNOWLEDGMENTS

This material is based upon work partly supported by NSF under Grant ECCS-1449270, AFOSR/NSF under EFRI 2-DARE Grant EFMA-1433459, and ARO under Gant W911NF-14-1-0572. J.M. acknowledges financial support from NSERC of Canada. The authors would like to thank Prof. Mark S. Lundstrom for valuable discussions.

■ REFERENCES

(1) Evans, K.; Alderson, A. *Adv. Mater.* **2000**, *12*, 617−628.
(2) Lakes, R. *Adv. Mater.* **1993**, *5*, 293−296.
(3) Love, A. *A treatise on the mathematical theory of elasticity*, 4th ed.; Cambridge University Press: New York, 1944.
(4) Lakes, R. *Science* **1987**, *235*, 1038−1040.
(5) Masters, I.; Evans, K. *Composite structures* **1996**, *35*, 403−422.
(6) Friis, E.; Lakes, R.; Park, J. *J. Mater. Sci.* **1988**, *23*, 4406−4414.
(7) Lakes, R. *J. Mater. Sci.* **1991**, *26*, 2287−2292.
(8) Evans, K.; Nkansah, M. A.; Hutchinson, I. J.; Rogers, S. C. *Nature* **1991**, *353*, 124.
(9) Prall, D.; Lakes, R. *Int. J. Mech. Sci.* **1997**, *39*, 305−314.
(10) Hall, L.; et al. *Science* **2008**, *320*, 504−507.
(11) Gunton, G.; Saunders, G. *J. Mater. Sci.* **1972**, *7*, 1061−1068.
(12) Li, Y. *Phys. Status Solidi A* **1976**, *38*, 171−175.
(13) Baughman, R.; Shacklette, J.; Zakhidov, A.; Stafstrom, S. *Nature* **1998**, *392*, 362−365.
(14) Milstein, F.; Huang, K. *Phys. Rev. B: Condens. Matter Mater. Phys.* **1979**, *19*, 2030−2033.
(15) Yeganeh-Haeri, A.; Weidner, D.; Parise, J. *Science* **1992**, *257*, 650−652.
(16) Keskar, N.; Chelikowsky, J. *Nature* **1992**, *358*, 222−224.
(17) Ho, D.; Park, S.; Kwon, S.; Park, K.; Kim, S. *Nat. Commun.* **2014**, *5*, 3255.
(18) Baughman, R. H.; Galvao, D. S. *Nature* **1993**, *365*, 735−737.
(19) Gaspar, N.; Ren, X.; Smith, C.; Grima, J.; Evans, K. *Acta Mater.* **2005**, *53*, 2439−2445.
(20) Morita, A. *Appl. Phys. A: Solids Surf.* **1986**, *39*, 227−242.
(21) Liu, H.; Du, Y.; Deng, Y.; Ye, P. D. *Chem. Soc. Rev.* **2015**, *44*, 2732−2743.
(22) Li, L.; et al. *Nat. Nanotechnol.* **2014**, *9*, 372−377.
(23) Liu, H.; et al. *ACS Nano* **2014**, *8*, 4033−4041.
(24) Xia, F.; Wang, H.; Jia, Y. *Nat. Commun.* **2014**, *5*, 4458.
(25) Li, L.; Kim, J.; Jin, C.; Ye, G.; Qiu, D. Y.; da Jornada, F. H.; Shi, Z.; Chen, L.; Zhang, Z.; Yang, F.; et al. Direct Observation of Layer-Dependent Electronic Structure in Phosphorene. **2016**, *arXiv:1601.03103*. arXiv.org e-Print archive. http://arxiv.org/abs/1601.03103 (accessed August 29, 2016).

DOI: 10.1021/acs.nanolett.6b03607
Nano Lett. 2016, 16, 6701−6708

(26) Wang, X.; et al. *Nat. Nanotechnol.* **2015**, *10*, 517−521.
(27) Koenig, S.; Doganov, R.; Schmidt, H.; Castro Neto, A.; Özyilmaz, B. *Appl. Phys. Lett.* **2014**, *104*, 103106.
(28) Castellanos-Gomez, A.; et al. *2D Mater.* **2014**, *1*, 025001.
(29) Luo, Z.; Maassen, J.; Deng, Y.; Du, Y.; Lundstrom, M.; Ye, P. D.; Xu, X.; Garrelts, R. P. *Nat. Commun.* **2015**, *6*, 8572.
(30) Rodin, A. S.; Carvalho, A.; Castro Neto, A. H. *Phys. Rev. Lett.* **2014**, *112*, 176801.
(31) Fei, R.; Yang, L. *Nano Lett.* **2014**, *14*, 2884−2889.
(32) Peng, X.; Wei, Q.; Copple, A. *Phys. Rev. B: Condens. Matter Mater. Phys.* **2014**, *90*, 085402.
(33) Cakir, D.; Sahin, H.; Peeters, F. M. *Phys. Rev. B: Condens. Matter Mater. Phys.* **2014**, *90*, 205421.
(34) Wei, Q.; Peng, X. *Appl. Phys. Lett.* **2014**, *104*, 251915.
(35) Kou, L.; Ma, Y.; Smith, S. C.; Chen, C. *J. Phys. Chem. Lett.* **2015**, *6*, 1509−1513.
(36) Jiang, J.; Park, H. *Nat. Commun.* **2014**, *5*, 4727.
(37) Fei, R.; Yang, L. *Appl. Phys. Lett.* **2014**, *105*, 083120.
(38) Wang, Y.; Cong, C.; Fei, R.; Yang, W.; Chen, Y.; Cao, B.; Yang, L.; Yu, T. *Nano Res.* **2015**, *8*, 3944−3953.
(39) Li, Y.; Hu, Z.; Lin, S.; Lai, S. K.; Ji, W.; Lau, S. P. *Adv. Funct. Mater.* **2016**, DOI: 10.1002/adfm.201600986.
(40) Conley, H.; et al. *Nano Lett.* **2013**, *13*, 3626−3630.
(41) Ni, Z.; et al. *ACS Nano* **2008**, *2*, 2301−2305.
(42) Ling, X.; et al. *Nano Lett.* **2015**, *15*, 4080−4088.
(43) Luo, X.; Lu, X.; Koon, G. K. W.; Castro Neto, A. H.; Ozylimaz, B.; Xiong, Q.; Quek, S. Y. *Nano Lett.* **2015**, *15*, 3931−3938.
(44) Harrison, W. A. *Elementary Electronic Structure*; World Scientific: Singapore, 1999.
(45) Jiang, J.; Chang, T.; Guo, X.; Park, H. *Nano Lett.* **2016**, *16*, 5286−5290.
(46) Jiang, J.; Park, H. *Nano Lett.* **2016**, *16*, 2657−2662.
(47) Shulenburger, L.; Baczewski, A. D.; Zhu, Z.; Guan, J.; Tománek, D. *Nano Lett.* **2015**, *15*, 8170−8175.
(48) Hu, Z. X.; Kong, X.; Qiao, J.; Normand, B.; Ji, W. *Nanoscale* **2016**, *8*, 2740−2750.
(49) Yang, L.; Cui, X.; Zhang, J; Wang, K.; Shen, M.; Zeng, S.; Dayeh, S. A.; Feng, L.; Xiang, B. *Sci. Rep.* **2014**, *4*, 5649.
(50) Kresse, G.; Furthmuller, J. *Phys. Rev. B: Condens. Matter Mater. Phys.* **1996**, *54*, 11169.
(51) Kresse, G.; Furthmuller, J. *Comput. Mater. Sci.* **1996**, *6*, 15−50.
(52) Kresse, G.; Joubert, D. *Phys. Rev. B: Condens. Matter Mater. Phys.* **1999**, *59*, 1758.
(53) Togo, A.; Tanaka, I. *Scr. Mater.* **2015**, *108*, 1−5.

DOI: 10.1021/acs.nanolett.6b03607
Nano Lett. 2016, 16, 6701−6708